Injury alters intrinsic functional connectivity within the primate spinal cord

Li Min Chen[a,b,c,1], Arabinda Mishra[a,b], Pai-Feng Yang[a,b], Feng Wang[a,b], and John C. Gore[a,b,d,e,f]

[a]Institute of Imaging Science and Departments of [b]Radiology and Radiological Sciences, [c]Psychology, [d]Biomedical Engineering, [e]Physics and Astronomy, and [f]Molecular Physiology and Biophysics, Vanderbilt University, Nashville, TN 37232

Recent demonstrations of correlated low-frequency MRI signal variations between subregions of the spinal cord at rest in humans, similar to those found in the brain, suggest that such resting-state functional connectivity constitutes a common feature of the intrinsic organization of the entire central nervous system. We report our detection of functional connectivity within the spinal cords of anesthetized squirrel monkeys at rest and show that the strength of connectivity within these networks is altered by the effects of injuries. By quantifying the low-frequency MRI signal correlations between different horns within spinal cord gray matter, we found distinct functional connectivity relationships between the different sensory and motor horns, a pattern that was similar to activation patterns evoked by nociceptive heat or tactile stimulation of digits. All horns within a single spinal segment were functionally connected, with the strongest connectivity occurring between ipsilateral dorsal and ventral horns. Each horn was strongly connected to the same horn on neighboring segments, but this connectivity reduced drastically along the spinal cord. Unilateral injury to the spinal cord significantly weakened the strength of the intrasegment horn-to-horn connectivity only on the injury side and in slices below the lesion. These findings suggest resting-state functional connectivity may be a useful biomarker of functional integrity in injured and recovering spinal cords.

hand | spinal cord injury | resting state fMRI | monkey | cervical spinal cord

Resting-state functional connectivity (rsFC) has been widely used to identify and characterize neural circuits in the brain (1–3), and its presentation at various spatial scales and its changes with specific physiological conditions confirm its fundamental role in maintaining normal brain function (4, 5). More importantly, alterations of rsFC networks in various disease conditions have altered our view about the functional significance of spontaneous baseline neural activity (3). Two very recent reports of success in detecting intrinsic functional circuits in human spines using resting-state fMRI once more suggest that rsFC is a fundamental, common feature of the entire nervous system (6, 7).

Despite these exciting findings in human subjects, the functional and behavioral relevance of the intrinsic functional networks within the spine gray matter remains largely obscure, and there have been no previous reports attempting to understand their significance. One way to address this question is to manipulate the network and then examine how the network reacts to the manipulation. This type of approach is impossible to execute in humans but can be performed in nonhuman primates in a very well-controlled manner. Thus, this study aimed to better understand the functional and behavioral relevance of newly identified rsFC in the spinal cord by first determining whether similar intrinsic rsFC networks can be detected in the spinal cords of anesthetized monkeys. We also sought to determine the relationship between stimulus-evoked fMRI activation patterns and the intrinsic rsFC networks in the spine, and whether and how unilateral injury to the cord changes the pattern or strength of rsFC. To address the above-mentioned critical questions, we conducted our research in a well-established unilateral spinal cord injury (SCI) model (8, 9) and used high-resolution fMRI at high field (10, 11) and tracer histology to quantify resting-state networks.

Traumatic SCI is a devastating medical condition that disrupts neural pathways, can lead to severe sensory impairment and motor deficits, and generally severely impairs the quality of life of SCI patients (12). Considerable research efforts and clinical trials have been devoted to attempts to restore impaired spinal cord function by promoting regeneration of disrupted neural pathways (13) or developing effective functional electrical stimulations (14) that assist the regaining of sensation and motor control. However, there has long existed a need for objective, noninvasive metrics of the effects of interventions. To date, behavioral assessments have been the gold-standard outcome measures of interventions, in both animals and humans studies (15). The strength or pattern of intrinsic rsFC within the spine may be a more sensitive noninvasive indicator of the states of local circuits both within and across spinal segments. Quantification of the intrinsic functional connectivity within the spine before and after injury has considerable potential to be a more objective imaging biomarker of spinal cord functional integrity. The knowledge gained in this fMRI study should be valuable for directing the use of fMRI for evaluating clinical prognosis and the effectiveness of therapeutic interventions.

Results

Distinct fMRI Responses in Cervical Spinal Cord to Noxious Heat Versus Innocuous Touch Stimulation. We first examined whether tactile stimulus-evoked activation in the dorsal horn of the cervical spinal cord of small monkeys could be detected and localized with adequate sensitivity and spatial precision by fMRI. In response to an 8-Hz vibratory stimulation of distal finger pad of digit 2 (D2) of the left hand, significant focal fMRI activation clusters were detected predominately on the ipsilateral side (left) of the gray matter in the base of the left dorsal horn (LDH) in

Significance

This is the first study, to our knowledge, to demonstrate intrinsic functional connectivity within the spinal cords of monkeys, replicating and extending recent similar discoveries in humans. Our observations of spatially correlated patterns of MRI signals at rest indicate that neurons in different parts of the spinal horns show synchronized fluctuations in activity at rest just as found in the brain. Injury to the cord disrupts the integrity of this interhorn connectivity within and across spinal segments, showing these intrinsic correlations have functional relevance and mirror behavioral deficits in the injured monkeys. Quantification of the intrinsic functional connectivity within the spine after injury therefore has considerable potential as an imaging biomarker of spinal cord functional integrity, something long needed in clinical practice.
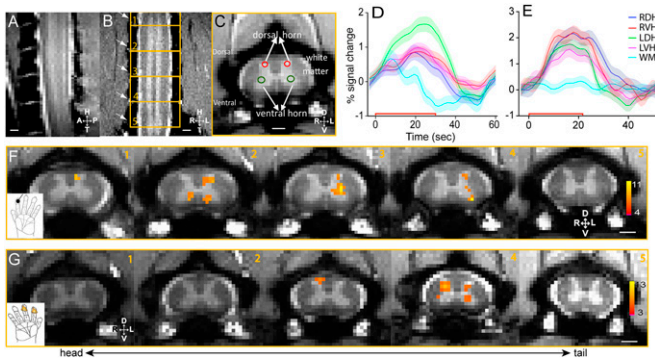
Fig. 1. Innocuous tactile and noxious heat stimuli evoked fMRI activations in the gray matter of cervical spinal cord. (*A*) Middle sagittal MTC image (0.75 mm thickness) of cervical spine showed the entering roots of C4–C7 afferents (white fiber bundles). (*B*) Coronal MTC image (0.5 mm thickness) shows the placement of five axial imaging slices, with the center slice at the C5/C6 level. Alternating white and gray (bright) matter strips of the spinal cord were apparent. Surrounding cerebrospinal fluid was present as two white strips on both the left and right sides of the spinal cord. Nerve afferents entering roots (indicated by white arrows) were also visible and allowed identification of each segment of the cervical spinal cord. (*C*) MTC axial image (3 mm thickness) revealed clearly the butterfly-shaped spinal gray matter. Red circles indicate the dorsal sensory horns, and green circles show the ventral horns. Surrounding back region comprises bone structures. (*D*) Event-averaged time courses of fMRI signal (%) to innocuous tactile (8 Hz vibration) stimulation at four horns (LDH, left dorsal horn; LVH, left ventral horn; RDH, right dorsal horn; RVH, right ventral horn) and one white matter (WM) control. The color shadow around each color line indicated the $\pm$SE of fMRI signal change. The red line along the *x* axis showed the 30-s stimulus duration. (*E*) Event-averaged time courses of fMRI signal (%) to noxious heat (47.5 °C) stimulation at four horns and one white matter control region. Stimulus duration is 21 s. (*F*) fMRI activation map to tactile stimulation of distal finger pad of D2 on left hand (thresholded at $t = 4$; see color scale bar in *5*) on five consecutive axial MTC structural images (*1–5*, from tail to head). (Black scale bar in *5*, 1 mm.) (*G*) fMRI activation map to noxious heat (47.5 °C) stimulation of distal finger pads of D2 and D3 on the right hand (thresholded at $t = 3$; see color scale bar in *5*). D, dorsal; L, left; R, right; V, ventral.

slices 2–4 (Fig. 1*F*), which correspond to the somatotopically appropriate cervical spinal segments of C5 and C6, which process afferent inputs derived from D3. The time course of fMRI signals (the average of six imaging runs) derived from the activation clusters in LDH on slices 2 and 3 showed robust $1.51 \pm 0.17\%$ (mean $\pm$ SE) signal changes (green line in Fig. 1*D*). In contrast, time courses derived from the other regions of the spinal cord (left ventral horn, LVH; right dorsal horn, RDH; right ventral horn, RVH) were weaker [see red ($0.81 \pm 0.12\%$), blue ($0.77 \pm 0.13\%$), and magenta ($0.62 \pm 0.19\%$) color lines in Fig. 1*D*], measureable but only about a half of that in LDH.

Noxious heat stimulation of the distal finger pads of D2 and D3 of the right hand elicited fMRI activations in bilateral dorsal–ventral horns and LVHs of C5 within a single slice (slice 4 in Fig. 1 *G*, *4*). Compared with the locations of tactile responses in the dorsal horn of the stimulated side (LDH in Fig. 1 *F*, *3*), the center of heat activation (RDH in Fig. 1 *G*, *4*) was located more dorsally toward the edge of the dorsal horn, corresponding to more superficial layers of the dorsal horn. The mean time courses calculated from each horn showed robust stimulus-evoked signal changes in all four horns (Fig. 1*E*), which were different from the tactile stimuli-evoked responses (Fig. 1*D*). The time courses in RDH ($1.91 \pm 0.20\%$) and RVH ($2.02 \pm 0.16\%$) were comparable (mean $\pm$ SE), whereas those in LDH (1.55 ± 0.14) and LVH (1.33 ± 0.16) were only slightly weaker (blue and magenta lines in Fig. 1*E*). As a control, the fMRI signal time course of adjacent white matter voxels showed negligible stimulus-related changes ($0.20 \pm 0.14\%$; blue line in Fig. 1*E*). The overall shape of the fMRI hemodynamic response function to noxious heat stimuli was very similar to those observed in early somatosensory

areas (16). The differential activation patterns and time courses of fMRI signals suggest that tactile and noxious heat inputs are likely processed by different spinal horns and functional circuits within the spinal cord gray matter.

Intrinsic Functional Connectivity Patterns of the Spinal Cord Horn. The observation of widespread activation in bilateral ventral and dorsal horns during the processing of noxious heat inputs suggests that spinal horns that are responsive to the same peripheral inputs may also be functionally connected. We therefore examined the regions of interest (ROIs)-based pair-wise correlation coefficients of resting-state fMRI signals among all four spinal horns and one randomly chosen white matter region, which served as a control ROI. For example, when a seed voxel was placed at the RVH in the third slice (Fig. 2*A*, yellow arrow on slice 3) in monkey SM-H, we observed a distinct functional connectivity pattern within and across image slices (correlation maps are thresholded at $r > 0.3$, $P < 10^{-5}$). Within each slice, the RVH was highly connected to all other horns (the LVH, RDH, and LDH). Also, across image slices, the RVH was highly connected to RVHs of other slices. Fig. 2*B* shows a similar functional connectivity pattern from a different monkey, SM-R (Fig. 2*B*). A seed at the LDH also exhibited a similar horn-to-horn correlation pattern (Fig. 2*D*). As a control, when the seed voxel was placed in the white matter, correlated voxels were detected only within the immediately adjacent white matter (Fig. 2 *C*, *3*).

The widespread functional connectivity pattern of a single horn was observed in all five animals studied. When the LVH
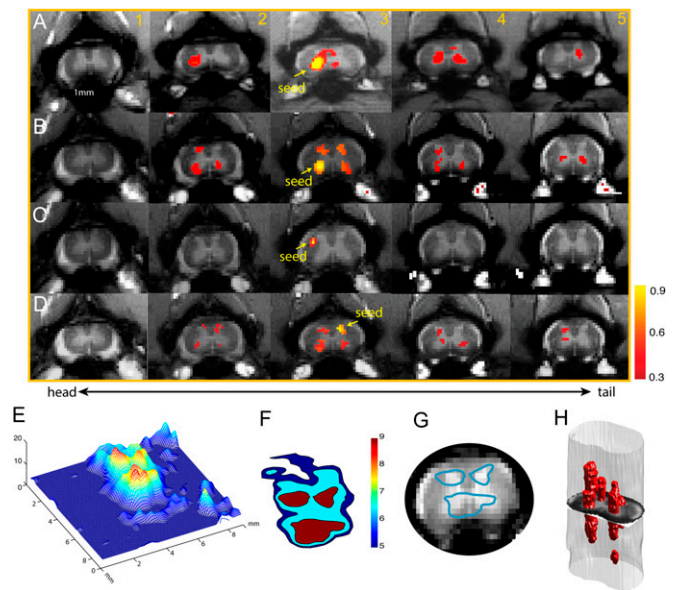

Fig. 2. Reproducible functional connectivity pattern of the spinal cord horns. (*A* and *B*) Intra- (within) and inter- (across) slice correlation patterns of the seeds (indicated by yellow arrows) placed at the ventral horns on slice 3 in two representative normal animals (*A*, SM-H; *B*, SM-R). Correlation maps were thresholded at $r > 0.30$ (see color scale bar next to image *5*). (*C*) Intra- and interslice correlation pattern of one control seed at the white matter of slice 3 in SM-H. (*D*) Intra- and interslice correlation patterns of the seed (indicated by yellow arrows) placed at the LDH on slice 3. Correlation maps were thresholded at $r > 0.30$ (see color scale bar next to image *5*). (*E*) A 3D illustration of the *t* statistic of the correlation map of the RVH at the group level (15 runs from 5 animals). (*F*) Corresponding contour map of the group correlation pattern at three different *t* statistics (blue, $t = 5$; light blue, $t = 6.5$; red, $t = 9$). The LVH in slice 3 in one subject was used as the point of interest for manual coregistration in the group analysis. (*G*) Overlay of the thresholded (red patch) correlation map of LVH seed on the mean intensity map of the spinal cord MTC images. (*H*) A 3D reconstruction of the correlation map from the sample case shown in *A*.

Chen et al.

www.manaraa.com

seeds on slice 3 were used to align all of the correlation maps across imaging runs and animals ($n = 5$ animals, a total of 15 runs), a strong horn-to-horn correlation pattern emerged (Fig. 2 *E–G*). A 3D view of the map of *t* statistics (calculated using manually coregistered correlation coefficient maps) revealed a fine-scale pattern within the spinal gray matter (Fig. 2*E*). In addition to the strong connectivity to other horns, there were three isolated local correlation peaks with the ventral horn seed. When we thresholded the group map at a *t* statistic > 9 (Fig. 2*F*) and overlaid the contours of the red patches (blue outline patches in Fig. 2*G*) with the structural image from one representative subject, it was clear that functional connectivity was robustly present among all four horns.

Differential Functional Connectivity Among Intraslice ROIs. We quantified the strengths of the resting-state correlations between different pairs of seed ROIs within each slice (intraslice) (Fig. S1). Representative 2D matrix plots from one subject show much stronger connectivity between horn–horn than horn–control ROI pairs regardless of the specific slice examined (Fig. S1*A* for slice 2 and Fig. S1*B* for slice 4). Whisker box plots of the group mean values and variations of correlation coefficients further support this observation (compare *1–4* with *5* and *6* columns in Fig. S1*C*). Furthermore, the ventral and dorsal horns on the same side exhibited the strongest connectivity (Fig. S1 *C*, *3*). Together, our data show that within a spinal cord segment (reflected by intraslice measures) spinal cord gray matter horns are connected strongly to other horns, but the intrahorn connectivity varied in strength.

SCI Altered the Functional Connectivity Between Intraslice ROIs. We next examined whether and how injury to the cord alters functional connectivity. We created unilateral lesions at the C5 level (the entering zone for D2/D3 afferents) in two (monkey SM-G and SM-P) of the five monkeys after baseline resting-state data had been collected. We centered the middle axial image slice (slice 3) at the midlesion level (Fig. 3 *C*, *1*). This image acquisition scheme allowed separate quantification of the pair-wise correlation coefficients of intraslice ROIs for slices 1 and 2 (above) and slices 4 and 5 (below) of the lesion (Fig. 3). The spatial extent and level of the lesion were later validated by histological examination of postmortem tissue (Fig. 3 *C*, *2* and *3*). Quantification of functional connectivity between ROIs within each slice led to three new findings.

First, within each slice, regardless of the positions above or below the lesion, the patterns of functional connectivity between ROIs within any slice were similar to those in normal conditions. For example, the 2D matrix plots of ROI correlations in two image slices (one below lesion, Fig. 3*A*, and one above lesion, Fig. 3*B*) from one representative subject show that the strongest correlations were between RDH and RVH. At the group level, this observation was confirmed (Fig. 3 *D* and *E*). Comparisons of the connectivity of ROI horns in pre- and postlesion conditions showed significantly reduced correlation coefficients (Fig. 3 *F*, *1–4*), indicating that intraslice horn–horn connectivity in slices below the lesion was significantly weakened after the injury. The dorsal horn–control ROI correlations were not affected, whereas ventral horn–control correlations were reduced (Fig. 3 *F*, *5* and *6*).
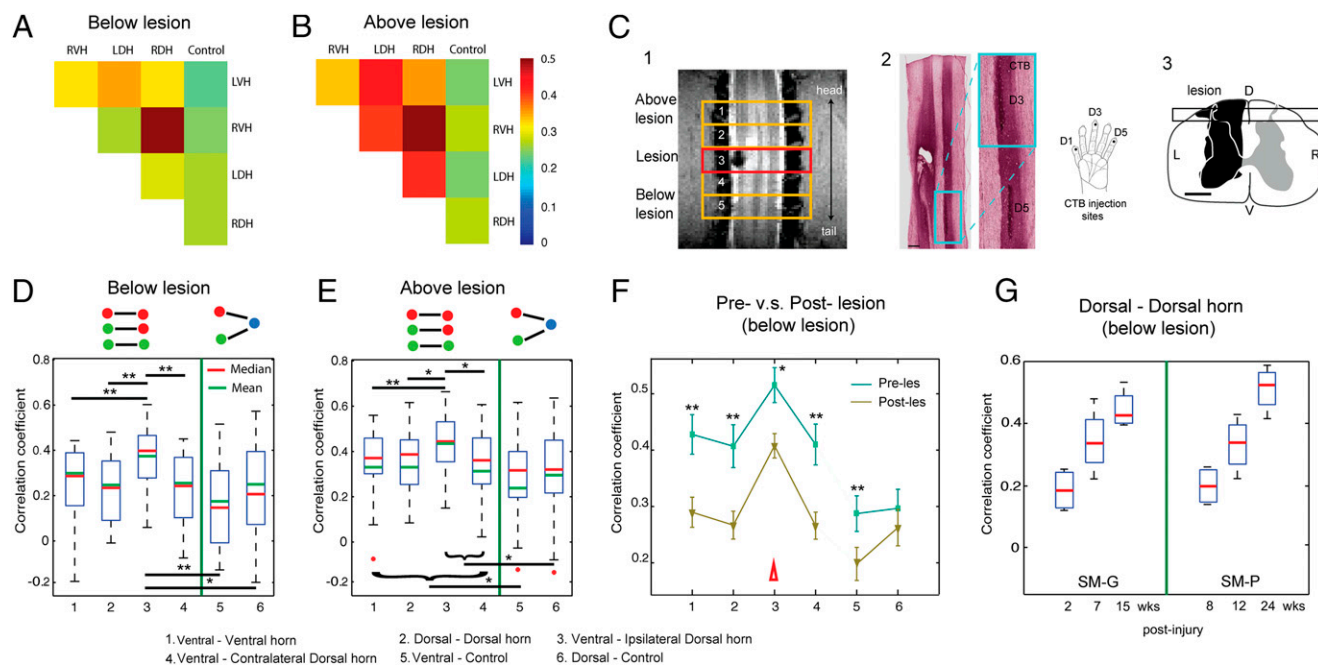
Fig. 3. Effects of a unilateral spinal cord lesion on the functional connectivity of intraslice ROIs. (*A* and *B*) The 2D matrix plots of the mean correlation coefficients (*r* values) among all five intraslice ROI pairs in below (*A*) and above (*B*) lesion slices in one representative animal (SM-P). The color bar indicates the range of *r* values. (*C*, *1*) Coronal MTC image shows the actual lesion (black hole) detected at the 2-week postlesion time point. Red rectangle outline shows the placement of the third axial image slice, which is centered at the lesion level. (*C*, *2*) CTB stain of the corresponding postmortem spinal cord obtained at 10 weeks after the lesion. Zoomed-in image (left) shows the CTB terminals of the afferent entering zone for D5 and D3. (*C*, *3*) The reconstructed lesion on the axial plane of the spinal cord in monkey SM-P. Black rectangle outline shows the location of the coronal MRI image shown in *2*. (*D* and *E*) Whisker box plots of the correlation coefficients between horn–horn ROI (columns *1–4*) and horn–control (white matter) ROI pairs (columns *5–6*) at the below lesion (slices 5 and 6) and above lesion (slices 1 and 2) imaging slices, respectively. Green lines separate the horn–horn and horn–control ROI pair groups. (*F*) Direct comparison of the mean correlation coefficients of the same set of ROI pairs obtained before (prelesion, green line) and after (postlesion, yellow line) the lesions. Error bars indicated the SD of the measurements. Datasets of 10 runs from two monkeys with spinal cord lesion acquired within 2–24 weeks postlesion were included in this analysis. (*G*) Whisker box plot of the correlation coefficients between dorsal–dorsal horns in below lesion slices as a function of postlesion time point (in weeks) in two injury monkeys (SM-G and SM-P).

Chen et al.

www.manaraa.com

Second, when we split the postlesion results and plotted the correlation coefficient (r value) as a function of time after injury, we observed a continuous trend in recovery of functional connectivity between dorsal and dorsal horns in slices below the lesions, as indicated by increasing r values in two subjects (Fig. 3G).

Finally, we separately examined how the functional correlations differed for horns that were ipsilateral or contralateral to the site of injury and compared their correlation values from slices above and below the lesions and in normal versus injured conditions (Fig. S2). We found that the effects of the lesions were unilateral and limited to the lesion side (the left side) in slices only below the injury (slices 4 and 5 in Fig. S2). For example, the correlation coefficient between the ventral–dorsal horns on the lesion (left) side in below lesion slices was significantly smaller than that on the contralateral (right) side (compare the two red columns in the right column group in Fig. S2). The correlation coefficients between the ventral to dorsal horn connections on both lesion and intact normal sides (left and right) in slices above the injury were greater than those of the lesion side below the lesion (compare the two red columns in the left group with the first red column in the right group in Fig. S2). Together, these observations indicate that the lesion reduced the functional connectivity only for horns on the lesion side and in spinal segments below the injury.

Histological Postmortem Confirmation of the Extent and Level of Each Injury. We used histology to confirm the spatial extent and location of each lesion. An example of an MRI image of a lesion and the corresponding histological cholera toxin subunit B (CTB)-stained section are shown in Fig. 3 C, 2, which confirmed the location as between the C4 and C5 level and in the rostral portion of the left D3 afferent entrance zone. For each digit, the afferent entrance zone spread ~2.5 mm along a rostral-to-dorsal direction along the cord (17). In no animal did the injury extend to the contralateral side of the spinal cord. More details of the histology are provided in *SI Results*.

SCI Altered the Functional Connectivity of ROIs Along the Cord. The spinal cord is organized in segments, each of which receives spatially specific inputs originating from different parts of the body. This somatotopic organization is a key feature for spatial encoding of peripheral information. We examined how far along the spinal cord the gray matter horns are functionally connected in normal conditions and how many segments are affected by a lesion by quantifying the strength of functional connection changes as a function of distance between ROI seeds along the spinal cord. We measured the correlation coefficients (r values) across corresponding ROI seed pairs, which were one to three imaging slices away (Fig. 4A). We found that voxels within the ROI seed at the LVH of slice 3 correlated strongly with its immediate neighboring voxels (self-correlation within the ROI, ~$r = 0.85$) (Fig. 4C). When the distance between the two ventral horn ROI seeds increased from one slice away (between slices 3 and 2 or slices 3 and 4) to two slices away (between slices 3 and 5 or slices 3 and 1), the connectivity strengths dropped markedly to ~$r = 0.4$ and below $r = 0.3$, respectively. This bell-shaped spatial correlation profile indicates that the functional connectivity along the spinal cord is spatially constrained to two spinal segments in normal conditions. After injury to the dorsal side of the spinal cord, the functional connectivity between ventral horn ROIs on two neighboring image slices below the lesion was significantly weakened (Fig. 4F). This finding indicates that unilateral spinal cord lesions not only reduced the functional connectivity among gray matter horns within each spinal segment but also weakened the connectivity between gray matter horns along the cord (across spinal segments).

Schematic Summary of the fMRI Findings in Both Normal and Lesion Conditions. Fig. 5 summarizes the main findings of the present study. In a normal spinal cord (Fig. 5A), gray matter horns within
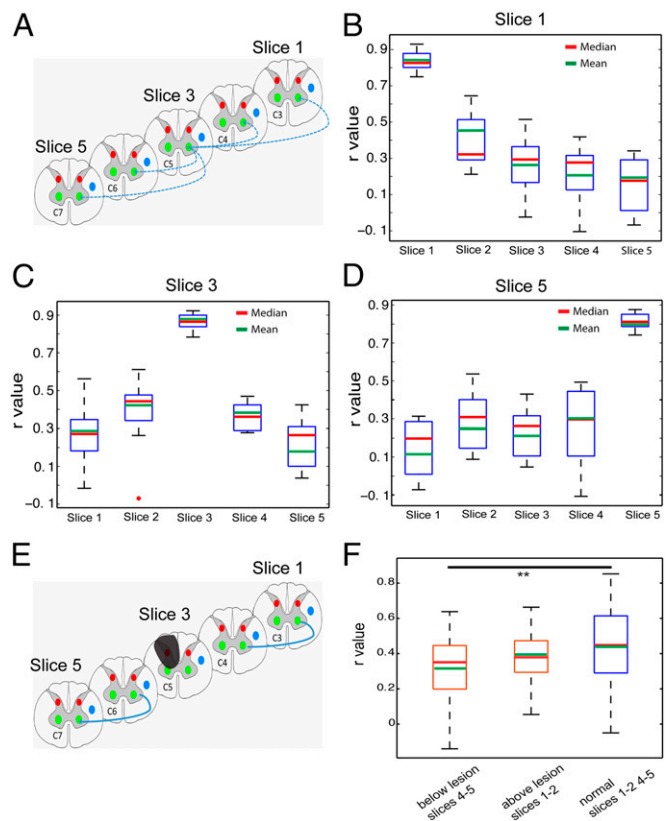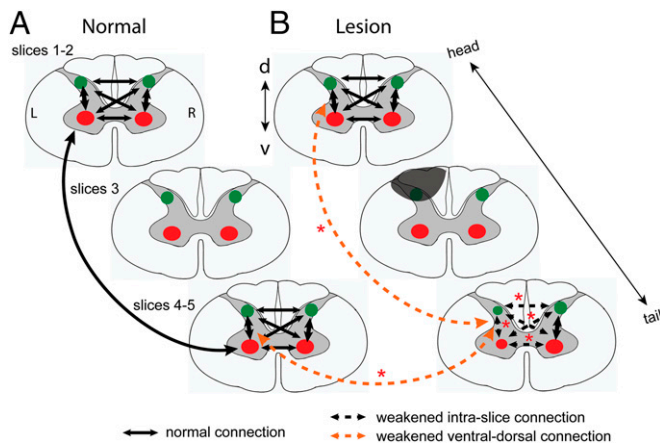

Fig. 4. Functional connectivity pattern of interslice ROIs in normal and lesion conditions. (*A*) Schematic diagram shows the pair-wise correlation analysis (indicated by blue lines) with respect to one particular seed ROI of the LVH of slice 3 (~ at C5 level). Correlation coefficients (r values) were calculated between the LVH on slice 3 (seed) with respect to the corresponding LVH on slices 1, 2, 4, and 5. (*B*) Whisker box plots of the correlation coefficient of the LVH ROI (on image slice 1) with other ventral horn seeds on slices 1–5 in the group analysis. (*C* and *D*) Whisker box plots of the correlation coefficients of the LVH seeds on the third (*C*) and fifth (*D*) slices with other ventral horn seeds. The upper and lower bounds of the box indicate the upper and lower quartile of the group data (15 datasets from 5 animals). The red and green lines indicate the mean and median values, respectively. (*E*) Schematic diagram shows the calculation scheme for comparing correlation values between interslice ROIs in lesion condition. Only correlations between corresponding horns (left ventral to left ventral) are included in the quantification. (*F*) Whisker box plots of r values in three different ROI pair groups: below lesion slices (between slices 4 and5), above lesion slices (between slices 1 and 2), and normal condition (between slices 1 and 2 and 4 and 5). **$P < 0.0001$ in Mann–Whitney Wilcoxon test.

each spinal segment are differentially connected. The strongest functional connectivity occurred between ipsilateral ventral and dorsal horns on the same side of the spinal cord. Gray matter horns are also strongly connected across spinal segments along the cord in a spatially constrained manner. Unilateral SCI, however, weakened the functional connectivity between gray matter horns on the lesion side within and across spinal segments below the lesion (Fig. 5B). The functional connectivity of inter- and intraslice horns in the slices above the lesion is comparable to those in a normal spinal cord.

Discussion

Widespread fMRI Responses to Noxious Stimuli Within Spinal Cord Gray Matter. Highly lateralized, somatotopic, and laminar-specific processing of nociceptive and innocuous tactile afferent inputs in the ipsilateral dorsal horn of the spinal cord is a fundamental feature of fine-scale local functional organization. The establishment of local intra- and intersegment circuitries has

www.manaraa.com

Fig. 5. Schematic illustration of the changes of functional connectivity between intra- and interslice ROIs after unilateral dorsal column lesion. (*A*) Functional connectivity patterns among horns within (intraslice) and across (interslice) imaging slices. The thickness (3 mm) of each slice approximately equals to the thickness of the single spinal cord segment. Green dots, dorsal horns; red dots, ventral horns. Black arrows indicate the functional connections, with thicker lines (ventral to dorsal) showing stronger connectivity. L, left side (lesion side); R, right side. (*B*) Altered functional connection patterns after unilateral lesion of the spinal cord gray and white matters. Gray shadow indicates the lesion. Dotted arrow lines indicate the weakened functional connectivity between different pairs of ROIs. Red asterisks represent the statistical significance level of the changes. Experimental results supporting the weakened ventral–dorsal horn connections (orange dotted lines) are presented in Fig. S2. *$P < 0.01$. d, dorsal; v, ventral. L, left; R, right.

been mainly based on studies in animals (18). In this noninvasive functional imaging study in nonhuman primates, our findings confirmed the presence of distinct neural circuits, but our results challenge the view of high degree of lateralization.

Nociceptive heat and tactile inputs are processed in a layer-specific manner in the ipsilateral dorsal horn (19, 20). By taking advantage of high-contrast and high-resolution MR images, we were able to clearly visualize and separate the butterfly-shaped gray matter from white matter. This permitted an accurate localization and delineation of the nociceptive stimuli-evoked fMRI responses to the more superficial portion of the dorsal horns and the tactile stimuli-evoked activity to the deeper part of the dorsal horn (Fig. 1). This layer-specific processing scheme for nociceptive heat and tactile inputs is consistent with findings reported from ex vivo animal studies (for a review, see ref. 21).

Stimulus-evoked fMRI responses were also detected in somatotopically appropriate spinal segments. Stimulations of the distal finger pads of D2 and D3 evoked fMRI activation in C5 to C6 segments (8, 17). Subsequent CTB tracer studies in these animals confirmed that the spinal segments in which fMRI activations were detected indeed receive input afferents from those digits. These observations confirmed that spinal fMRI activations were somatotopically organized along the cord.

Finally and most interestingly, we found that the unilateral nociceptive and tactile stimuli evoked much more widespread fMRI activations in all four horns. Ventral horn activation to nociceptive stimuli can be explained by the coactivation of local spinal reflex circuitry. However, the ventral horn activations to tactile stimulation suggest that ventral horns likely play a larger role than mediating simple reflexes associated with nociceptive stimuli. Our observations indicate at least that the processing of nociceptive and tactile inputs actually engages a much more complex spinal circuitry than previously recognized. The fMRI activation in contralateral dorsal horns has been reported in human spinal fMRI studies, but the results so far have been inconsistent with respect to which horn is engaged in pain versus touch processing, partly due to the relatively low spatial resolution in conventional human 3T MRI studies (22, 23) (for recent

reviews, see refs. 24, 25). The contralateral dorsal horn activation we detected may be a result of feedback-descending modulation (20, 21) or from commissural connections between dorsal horns (26). Our demonstration of bilateral dorsal and ventral horn activations in response to unilateral nociceptive and tactile stimuli in anesthetized monkeys speaks strongly for the fundamental importance of the circuitry among the four horns.

Correlation Between Stimulus-Driven Activation Pattern and rsFC and Its Functional Relevance. A large body of literature supports the concept that in the brain, regions that are engaged together in processing external stimuli also exhibit strong rsFC (3–5, 27–29). External sensory inputs further interact with this baseline state, resulting in various network modulations. For example, within the S1 cortex, we found previously that rsFC is highly correlated in time and space, with underlying synchronized unit electrophysiological activity and intrinsic anatomical connections between corresponding regions representing distal finger pads (5). The current study extends these ideas from the brain to the spinal cord. Our findings indicate that baseline functional connectivity is a common organizational feature within the central nervous system (6, 7, 30). Spinal gray matter horns are highly functionally connected at rest, to a much greater degree than has been previously recognized. Strong dorsal horn-to-horn connectivity was found in our study in anesthetized monkeys as well as in the two very recent studies in awake humans using different analytic methods (6, 7). However, the specific horn-to-horn functional connectivity patterns within and across segments varied from the current study. This variation may be attributed to at least three factors. The first could be the increased signal-to-noise ratio at high field, which improves the detection of functional connections between horns even under anesthesia (5, 31). The second may relate to functional organizational differences across species because monkeys use more coordinated bilateral locomotor behaviors than humans. The third factor could be the anesthesia, which is known to reduce the measured strengths of functional connectivity in an area-dependent manner (32, 33). However, studies have shown that anesthesia has a significantly weaker influence in early sensory cortical areas and very likely in the downstream spinal cord than higher order cognitive brain regions (for a review, see ref. 34). We believe that anesthesia is unlikely a major influence on the horn-to-horn connectivity differences between anesthetized monkeys and awake humans (4, 5) or before and after injury. Taken together, the spinal resting-state connectivity circuits, just like those in the brain, likely provide a baseline network configuration upon which external or descending inputs are further processed, such as during coordinated left and right activity and/or sensory and motor integrations (19, 35). Alterations in these resting-state networks, such as after injury to the spinal cord, may set a completely different basis for the processing of external sensory or motor inputs.

Functional Relevance of the Resting-State Network in the Spine. We identified rsFC networks among spinal horns in normal conditions and then found postinjury that the integrity of local circuits on one side was disrupted. We found that unilateral injury altered the functional connectivity between intraslice horns only in the spinal segments below the lesion and that the functional connectivity of the dorsal and ventral horns on the side of the injury was significantly weakened. By contrast, the ventral–dorsal horn connectivity on the opposite uninjured side remained strong, at a level comparable to that in normal conditions. These two main observations indicate that top–down descending activity may be a significant driving force of the interhorn connectivity (36, 37). When this common drive was disrupted by injury, correlated rsFC signals between horns were reduced. The strongest connectivity between the ipsilateral ventral and dorsal horns may represent an underlying functional framework for a more lateralized information processing in the spinal cord of new world monkeys. Given the fact that lateralization and somatotopic processing of afferent inputs are fundamental encoding

Chen et al.

APPLIED BIOLOGICAL SCIENCES

features of the spinal cord, the selective alteration of spinal horn connectivity after SCI further supports the functional relevance of rsFC among the horns. Thus, the rsFC pattern may be a potential marker of the integrity of neural processing.

In summary, this article describes, for the first time (to our knowledge), the use of high-field MRI to detect and delineate functional circuits within the spinal cord of nonhuman primates and how they change as a result of injury to the cord. The identification of functionally connected networks within the brain using fMRI in a resting state has dramatically improved our understanding of the functional circuits that belie specific brain functions. This study extends those observations from the brain to the spinal cord, where we identify intrinsic local functional connectivity networks within and across spinal segments. We observed differential fMRI activation patterns to tactile versus nociceptive heat stimuli within a single spinal segment, and these stimuli-evoked interhorn activation patterns were similar to the resting-state interhorn functional connectivity pattern. These observations indicate that neurons in the spinal sensory and motor horns fire together when stimulated and fluctuate together at rest. Furthermore, we discovered that unilateral injury to the spinal cord alters the connectivity within these intrinsic intra- and interspinal segment circuitries. Given the known behavioral consequences of SCI on monkey sensory–motor behavior in this model, the effects of injury further support the functional relevance of the MRI findings. The clear trend of functional connectivity recovery between bilateral dorsal horns after injury illustrates the potential of rsFC as a prognostic indicator to monitor certain behavioral impairments. In practice, such functional and quantitative imaging data can be acquired early after the injury is produced and repeated weekly. This permits serial evaluation of functional and structural changes during recovery and direct correlation with behavioral data obtained from each animal. Thus, quantification of the intrinsic functional connectivity within the spine before and after injury has considerable potential to be an imaging biomarker of spinal cord functional integrity, something that has long been needed in clinical practice.

Materials and Methods

Animal Preparation. Five adult (6–8 y old) male squirrel monkeys (*Saimiri sciureus*) were included in this study. All procedures were approved by Institutional Animal Care and Use Committees at Vanderbilt University. Details of their treatment are provided in *SI Materials and Methods*.

In Vivo MRI Data Acquisition and Analysis. MRI scans were performed on an Agilent 9.4T scanner using a saddle-shaped transmit–receive surface coil (2.5 × 3 cm² in size) positioned over the animal's neck. Five contiguous axial slices (each 3 mm in thickness), with the third slice positioned over the C5 segment (where the lesion was later targeted in two animals), were acquired in each imaging session. High-resolution structural images with Magnetization Transfer Contrast (MTC) were acquired before functional images. Details of the fMRI data acquisition protocol are described in *SI Materials and Methods*. The preprocessing and an ROI-based correlation analysis of fMRI data were conducted with customized software in SPM5/8. For detailed information, see *SI Materials and Methods*.

1. Biswal B, Yetkin FZ, Haughton VM, Hyde JS (1995) Functional connectivity in the motor cortex of resting human brain using echo-planar MRI. *Magn Reson Med* 34(4):537–541.
2. Fox MD, Corbetta M, Snyder AZ, Vincent JL, Raichle ME (2006) Spontaneous neuronal activity distinguishes human dorsal and ventral attention systems. *Proc Natl Acad Sci USA* 103(26):10046–10051.
3. Fox MD, Greicius M (2010) Clinical applications of resting state functional connectivity. *Front Syst Neurosci* 4:19.
4. Vincent JL, et al. (2007) Intrinsic functional architecture in the anaesthetized monkey brain. *Nature* 447(7140):83–86.
5. Wang Z, et al. (2013) The relationship of anatomical and functional connectivity to resting-state functional connectivity in primate somatosensory cortex. *Neuron* 78(6):1116–1126.
6. Barry RL, Smith SA, Dula AN, Gore JC (2014) Resting state functional connectivity in the human spinal cord. *eLife* 3:e02812.
7. Kong Y, et al. (2014) Intrinsically organized resting state networks in the human spinal cord. *Proc Natl Acad Sci USA* 111(50):18067–18072.
8. Qi HX, Chen LM, Kaas JH (2011) Reorganization of somatosensory cortical areas 3b and 1 after unilateral section of dorsal columns of the spinal cord in squirrel monkeys. *J Neurosci* 31(38):13662–13675.
9. Yang PF, Qi HX, Kaas JH, Chen LM (2014) Parallel functional reorganizations of somatosensory areas 3b and 1, and S2 following spinal cord injury in squirrel monkeys. *J Neurosci* 34(28):9351–9363.
10. Hutchison RM, Everling S (2012) Monkey in the middle: Why non-human primates are needed to bridge the gap in resting-state investigations. *Front Neuroanat* 6:29.
11. Harel N (2012) Ultra high resolution fMRI at ultra-high field. *Neuroimage* 62: 1024–1028.
12. Freund P, et al. (2011) Disability, atrophy and cortical reorganization following spinal cord injury. *Brain* 134(Pt 6):1610–1622.
13. Thuret S, Moon LD, Gage FH (2006) Therapeutic interventions after spinal cord injury. *Nat Rev Neurosci* 7(8):628–643.
14. Bamford JA, Mushahwar VK (2011) Intraspinal microstimulation for the recovery of function following spinal cord injury. *Prog Brain Res* 194:227–239.
15. Goldberger ME, Bregman BS, Vierck CJ, Jr, Brown M (1990) Criteria for assessing recovery of function after spinal cord injury: Behavioral methods. *Exp Neurol* 107(2): 113–117.
16. Chen LM, et al. (2007) High-resolution maps of real and illusory tactile activation in primary somatosensory cortex in individual monkeys with functional magnetic resonance imaging and optical imaging. *J Neurosci* 27(34):9181–9191.
17. Florence SL, Wall JT, Kaas JH (1991) Central projections from the skin of the hand in squirrel monkeys. *J Comp Neurol* 311(4):563–578.
18. Hultborn H (2006) Spinal reflexes, mechanisms and concepts: From Eccles to Lundberg and beyond. *Prog Neurobiol* 78(3-5):215–232.
19. Darian-Smith I (1982) Touch in primates. *Annu Rev Psychol* 33:155–194.
20. Willis WDJ, Coggeshall RE (2004) *Structure of the Dorsal Horn* (Kluwer Academic/ Plenum Publishers, New York).
21. Costigan M, Scholz J, Woolf CJ (2009) Neuropathic pain: A maladaptive response of the nervous system to damage. *Annu Rev Neurosci* 32:1–32.
22. Brooks JC, et al. (2012) Stimulus site and modality dependence of functional activity within the human spinal cord. *J Neurosci* 32(18):6231–6239.
23. Stroman PW, Bosma RL, Tsyben A (2012) Somatotopic arrangement of thermal sensory regions in the healthy human spinal cord determined by means of spinal cord functional MRI. *Magn Reson Med* 68(3):923–931.
24. Wheeler-Kingshott CA, et al. (2014) The current state-of-the-art of spinal cord imaging: Applications. *Neuroimage* 84:1082–1093.
25. Stroman PW, et al. (2014) The current state-of-the-art of spinal cord imaging: Methods. *Neuroimage* 84:1070–1081.
26. Petkó M, Antal M (2012) Propriospinal pathways in the dorsal horn (laminae I-IV) of the rat lumbar spinal cord. *Brain Res Bull* 89(1-2):41–49.
27. Deco G, et al. (2013) Resting-state functional connectivity emerges from structurally and dynamically shaped slow linear fluctuations. *J Neurosci* 33(27):11239–11252.
28. Cohen MR, Kohn A (2011) Measuring and interpreting neuronal correlations. *Nat Neurosci* 14(7):811–819.
29. Fox MD, Raichle ME (2007) Spontaneous fluctuations in brain activity observed with functional magnetic resonance imaging. *Nat Rev Neurosci* 8(9):700–711.
30. Smith SM, et al. (2009) Correspondence of the brain's functional architecture during activation and rest. *Proc Natl Acad Sci USA* 106(31):13040–13045.
31. Harel N (2012) Ultra high resolution fMRI at ultra-high field. *Neuroimage* 62(2): 1024–1028.
32. Jonckers E, et al. (2014) Different anesthesia regimes modulate the functional connectivity outcome in mice. *Magn Reson Med* 72(4):1103–1112.
33. Grandjean J, Schroeter A, Batata I, Rudin M (2014) Optimization of anesthesia protocol for resting-state fMRI in mice based on differential effects of anesthetics on functional connectivity patterns. *Neuroimage* 102(Pt 2):838–847.
34. Bonhomme V, et al. (2011) Influence of anesthesia on cerebral blood flow, cerebral metabolic rate, and brain functional connectivity. *Curr Opin Anaesthesiol* 24(5): 474–479.
35. Falgairolle M, de Seze M, Juvin L, Morin D, Cazalets JR (2006) Coordinated network functioning in the spinal cord: An evolutionary perspective. *J Physiol Paris* 100(5-6): 304–316.
36. Basso DM, Beattie MS, Bresnahan JC (2002) Descending systems contributing to locomotor recovery after mild or moderate spinal cord injury in rats: Experimental evidence and a review of literature. *Restor Neurol Neurosci* 20(5):189–218.
37. Parker D (2009) Descending interactions with spinal cord networks: A time to build? *J Physiol* 587(Pt 20):4761.